

Extragalactic Gas at Low Redshift
ASP Conference Series, Vol. , 2001
J. S. Mulchaey and J. T. Stocke

The Extragalactic Ionizing Background at Low Redshift

Jennifer Scott, Jill Bechtold, Miwa Morita

Steward Observatory, University of Arizona, Tucson, AZ 85721

Adam Dobrzański

*Harvard-Smithsonian Center for Astrophysics, 60 Garden Street,
Cambridge, MA 02138*

Varsha P. Kulkarni

*University of South Carolina, Department of Physics and Astronomy,
Columbia, SC 29208*

Abstract. We present a measurement of the mean intensity of the hydrogen-ionizing background radiation field at low redshift using 906 Ly α absorption lines in 151 quasar spectra from the archives of the Faint Object Spectrograph (FOS) on the Hubble Space Telescope (HST). Using a maximum likelihood technique and the best estimates possible for each QSO's Lyman limit flux and systemic redshift, we find $J(\nu_0) = 7.6_{-3.0}^{+9.4} \times 10^{-23}$ ergs s $^{-1}$ cm $^{-2}$ Hz $^{-1}$ sr $^{-1}$ at $0.03 < z < 1.67$. This is in good agreement with the mean intensity expected from models of the background which incorporate only the known quasar population. When the sample is divided into two subsamples, consisting of lines with $z < 1$ and $z > 1$, the values of $J(\nu_0)$ found are $6.5_{-1.6}^{+38.} \times 10^{-23}$ ergs s $^{-1}$ cm $^{-2}$ Hz $^{-1}$ sr $^{-1}$, and $1.0_{-0.2}^{+3.8} \times 10^{-22}$ ergs s $^{-1}$ cm $^{-2}$ Hz $^{-1}$ sr $^{-1}$, respectively, indicating that the mean intensity of the background is evolving over the redshift range of this data set. Relaxing the assumption that the spectral shapes of the sample spectra and the background are identical, the best fit HI photoionization rates are found to be 6.7×10^{-13} s $^{-1}$ for all redshifts, and 1.9×10^{-13} s $^{-1}$ and 1.3×10^{-12} s $^{-1}$ for $z < 1$ and $z > 1$, respectively.

1. Mean intensity of the UV Background

The maximum likelihood method for measuring $J(\nu_0)$ as presented by Kulkarni & Fall (1993, KF93) consists of constructing a likelihood function of the form

$$L = \prod_a f(N_a, z_a) \prod_Q \exp \left[- \int_{z_{min}^Q}^{z_{max}^Q} dz \int_{N_{min}^Q}^{\infty} f(N, z) dN \right], \quad (1)$$

where

$$f(N, z) = AN^{-\beta}(1+z)^\gamma[1+\omega(z)]^{-(\beta-1)}. \quad (2)$$

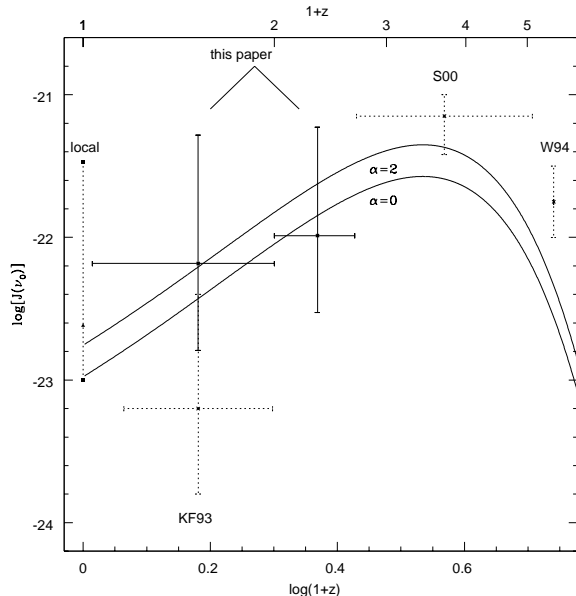


Figure 1. $\log[J(\nu_0)]$ versus redshift: (filled triangle)- Shull et al. (1999); (filled squares & dotted line)- limits from $\text{H}\alpha$ imaging; (crosses)- our results for $z < 1$ and $z > 1$; points with dotted error bars centered at $z \sim 0.6, 3, 4.5$ are results from KF93, Paper II, and Williger et al. (1994), respectively; (solid curves)- HM96 models for two values of the global source spectral index, α

Using the values of γ and A_0 from a separate maximum likelihood analysis, and a value of β from studies with high resolution data, eg. $\beta = 1.46$ from Hu et al. (1995), the search for the best-fit value of $J(\nu_0)$ consists of finding the value that maximizes this function, fixing the other parameters.

The models of Haardt & Madau (1996, HM96) predict that the UV background arising from QSOs drops by over an order of magnitude from $z = 2.5$ to $z = 0$. We therefore divide the sample into low and high redshift subsamples at $z = 1$ and solve for $J(\nu_0)$. These results, listed in Table 1. confirm some evolution in $J(\nu_0)$, though not at a high level of significance. The maximum likelihood analysis yields $\log[J(\nu_0)] = -22.18^{+0.90}_{-0.61}$ at $z < 1$ and $\log[J(\nu_0)] = -21.98^{+0.76}_{-0.54}$ at $z > 1$. These results are also shown in Figure 1.

Including associated absorbers, damped Ly α absorbers, or blazars in the proximity effect analysis has little effect on the results. One might expect associated absorbers to reduce the magnitude of the observed proximity effect and hence cause $J(\nu_0)$ to be overestimated. The value found including the 45 associated absorbers in our sample is indeed larger, $\log[J(\nu_0)] = -21.74^{+0.55}_{-0.39}$, versus $\log[J(\nu_0)] = -22.11^{+0.52}_{-0.40}$, but not significantly so. Likewise, if the intervening dust extinction in damped Ly α absorbers is significant, including these objects in our analysis could cause us to overestimate the magnitude of the proximity effect and hence underestimate $J(\nu_0)$. However, the inclusion of these 7 objects only negligibly reduces the value of $J(\nu_0)$ derived. QSO variability on timescales less than $\sim 10^5$ years would be expected to smooth out the proximity effect distribu-

Table 1. Measurements of $J(\nu_0)$

Sample ^a	\mathcal{N}_{lines}^b	γ, A	β	b	$\log[J(\nu_0)]$	Q_{KS}^c
1.....	259	0.8298, 6.73524	1.46	35	$-22.11^{+0.51}_{-0.40}$	0.80
1a.....	162	1.5082, 4.92095	1.46	35	$-22.18^{+0.90}_{-0.61}$	0.64
1b.....	97	-0.8702, 26.1886	1.46	35	$-21.98^{+0.76}_{-0.54}$	0.98
2.....	289	0.1502, 12.0134	1.46	35	$-22.03^{+0.44}_{-0.37}$	0.30

^aSample number- (1) All lines with $W > 0.32 \text{ \AA}$, (1a) $z < 1$, (1b) $z > 1$; (2) All lines with $W > 0.24 \text{ \AA}$

^bNumber of Ly α forest lines in sample

^cK-S probability

tion (Bajtlik, Duncan, & Ostriker 1988). However, the inclusion of 6 blazars in the sample, all at $z < 1$, resulted in no discernible change in $J(\nu_0)$. The sample used in the analysis of HI ionization rates discussed below includes all of these objects.

For each solution, we also execute a Kolmogorov-Smirnov (KS) test. The KS test provides a measure of how well the assumed parent distribution of lines with respect to redshift, given by Equation 2, reflects the true redshift distribution of lines. The KS probability, Q_{KS} , indicates the probability that a value of the KS statistic larger than the one calculated could have occurred by chance if the assumed parent is correct. The KS probability associated with each solution for $J(\nu_0)$ is listed in column 7 of Table 1.

2. HI Ionization Rate

Solving for the HI ionization rate,

$$\Gamma = \int_{\nu_0}^{\infty} \frac{4\pi J(\nu)\sigma_{HI}(\nu)}{h\nu} d\nu \text{ s}^{-1}, \quad (3)$$

instead of for $J(\nu_0)$ avoids the assumption that the spectral indices of the QSO and the background are identical. We modified our maximum likelihood code to conduct the search for this quantity and the results are listed in Table 2. Evolution in the UV background is more apparent in the HI ionization rate than in the solutions for $J(\nu_0)$. The result at $z > 1$ is 6.5 times larger than that at $z < 1$.

We also parametrize the evolution of the HI ionization rate as a power law:

$$\Gamma(z) = A(1+z)^B \quad (4)$$

and solve for the parameters A and B in both the constant and variable threshold cases. The values we find are also listed in Table 2 and plotted in Figure 2.

Table 2. HI Ionization Rates

Sample ^a	γ, A	β	b	$\log[\Gamma_{\text{HI}}]$
1.....	0.6925, 7.64986	1.46	35	-12.17 ^{+0.50} _{-0.40}
1a.....	0.8452, 7.10998	1.46	35	-12.70 ^{+0.74} _{-0.51}
1b.....	0.7209, 7.29421	1.46	35	-11.88 ^{+0.74} _{-0.50}
1.....	0.6925, 7.20637	1.46	35	-12.67, 1.73 ¹

^a(1) All lines with $W > 0.32 \text{ \AA}$, (1a) $z < 1$, (1b) $z > 1$

¹Maximum Likelihood solution for A,B (see §2, Equ. 4)

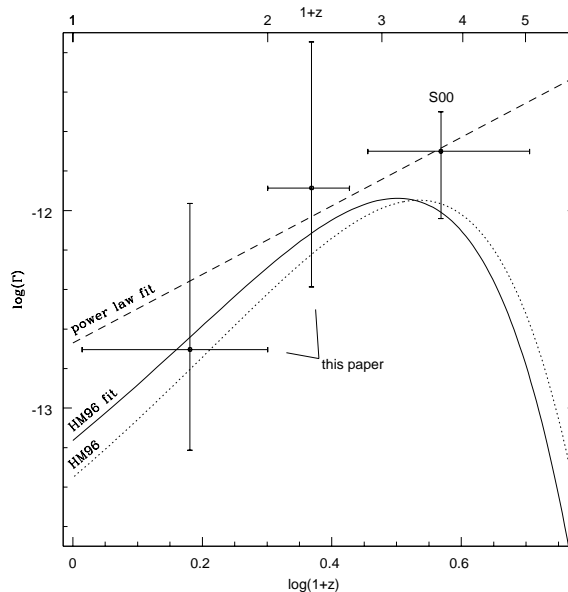


Figure 2. HI ionization rate versus redshift: (points)- constant equivalent width threshold maximum likelihood solutions from this paper, $z < 1$ and $z > 1$ and from Paper II for $1.7 < z < 3.8$; (dashed line)- Solution to Equ. 4 for HST/FOS data alone; (solid line)- Solution to Equ. 5 for HST/FOS data combined with high redshift data from Paper II, (dotted line)- HM96 solution to Equ. 5

HM96 parametrize their models of the HI ionization rate as a function of redshift:

$$\Gamma(z) = A(1+z)^B \exp\left(\frac{-(z-z_c)^2}{S}\right) \quad (5)$$

We combine our data set with that of Scott et al. 2000b (Paper II) to solve for the parameters A , B , z_c , and S . We find $(A, B, z_c, S) = (7.6 \times 10^{-13}, 0.35, 2.07, 1.77)$, while the HM96 parameters for $q_0 = 0.5$ are $(6.7 \times 10^{-13}, 0.43, 2.30, 1.95)$. These results are shown in Figure 2, and the HM96 parametrization is also shown for comparison.

3. Ly α forest line density

The number density evolution of Ly α absorbers over the redshift range $z = 0 - 5$ cannot be approximated with a single power law. There is a significant break in the slope of the line number density with respect to redshift, near $z \approx 1.7$. Davé et al. (1999) show from hydrodynamical simulations of the low redshift Lyman α forest, that the evolution of the line density is sensitive mainly to the HI photoionization rate, but also to the evolution of structure. The flattening of dN/dz observed by Weymann et al. (1998) is mostly attributed to a dramatic decline in $\Gamma(z)$ with decreasing z . Davé et al. (1999) derive an expression for the density of Lyman α forest lines per unit redshift as a function of the HI photoionization rate:

$$\frac{dN}{dz} = C[(1+z)^5 \Gamma_{\text{HI}}^{-1}(z)]^{\beta-1} H^{-1}(z), \quad (6)$$

where C is the normalization at some fiducial redshift which we choose to be $z = 0$ and $\Gamma(z)$ can be expressed by Equ. 5.

We fit the FOS and MMT absorption line data, binned in dN/dz , presented in Dobrzycki et al. (2001, Paper IV) and in Scott et al. (2000a, Paper I), to this function in order to derive the parameters describing $\Gamma(z)$ implied by the evolution in Lyman α forest line density. We observe some flattening of dN/dz at $z < 1.7$, but not to the degree seen by Weymann et al. (1998) in the Key Project data. We find $\gamma = 0.50 \pm 0.21$, for lines above a 0.24 \AA threshold (Paper IV), while Weymann et al. (1998) measure $\gamma = 0.15 \pm 0.23$. We find $(A, B, z_c, S) = (3.0 \times 10^{-12}, 0.61, 5.5 \times 10^{-7}, 7.07)$ and $(1.9 \times 10^{-11}, 0.38, 3.4 \times 10^{-7}, 6.21)$ for $(\Omega_M, \Omega_\Lambda) = (1, 0)$ and lines with rest equivalent widths above 0.24 and 0.32 \AA , respectively. These fits to Equ. 6 are shown in Figure 3(a). In panel (b), we plot $\Gamma(z)$, as expressed in Equ. 5, evaluated using the parameters found from the fit to Equ. 6 above. The HM96 solution and the solution derived from the full FOS and MMT data sets are represented by the thick and thin black lines respectively. The small values of z_c derived from dN/dz above translate into ionization rates that do not decrease dramatically with decreasing redshift and result from the less pronounced flattening of dN/dz relative to the Key Project. The observed $\Gamma(z)$ falls short of the ionization rate needed to fully account for the change in the Lyman α line density with redshift, indicating that the formation of structure in the low redshift universe plays a significant role in determining the character of the Ly α forest line density.

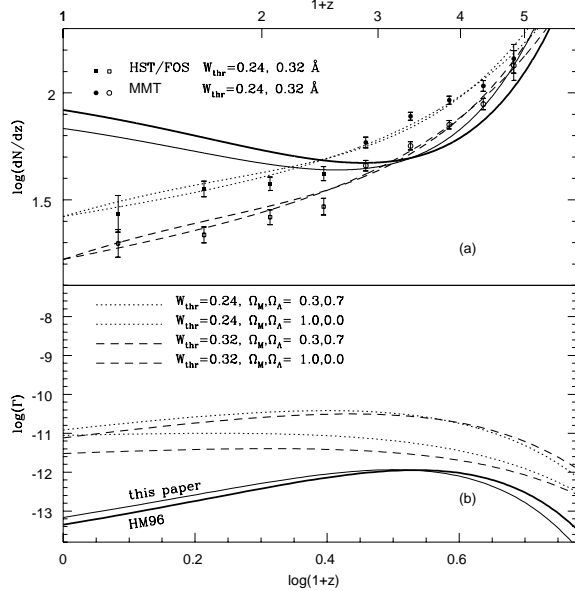


Figure 3. (a) dN/dz versus redshift: $W_{\text{thr}} = 0.24 \text{ \AA}$ with fit to Equ. 6 (solid points, dotted lines), $W_{\text{thr}} = 0.32 \text{ \AA}$ with fit to Equ. 6 (open points, dashed lines), Equ. 6 evaluated with HM96 parameters for $\Gamma(z)$ expressed by Equ. 5 (thick solid line), Equ. 6 evaluated with parameters for $\Gamma(z)$ found in this paper (thin solid line); (b) $\Gamma(z)$ versus redshift expressed by Equ. 5 using HM96 parameters (thick solid line), using parameters found in this paper (thin solid line), and using parameters found from fits to dN/dz for $W_{\text{thr}} = 0.24 \text{ \AA}$ and $(\Omega_M, \Omega_\Lambda) = (1.0, 0.0)$ (thin dotted line), $W_{\text{thr}} = 0.24 \text{ \AA}$ and $(\Omega_M, \Omega_\Lambda) = (0.3, 0.7)$ (thick dotted line), $W_{\text{thr}} = 0.32 \text{ \AA}$ and $(\Omega_M, \Omega_\Lambda) = (1.0, 0.0)$ (thin dashed line), and $W_{\text{thr}} = 0.32 \text{ \AA}$ and $(\Omega_M, \Omega_\Lambda) = (0.3, 0.7)$ (thick dashed line)

4. Summary of Results

We have analyzed a set of 151 QSOs and 906 Ly α absorption lines, the subset of the total data set presented in Paper III that is appropriate for the proximity effect. The primary results of this work are as follows:

- (1) The value of $J(\nu_0)$ is observed to increase with redshift over the redshift range of the sample data, $0.03 < z < 1.67$. Dividing the sample at $z = 1$, we find $J(\nu_0) = 6.5^{+38.}_{-1.6} \times 10^{-23} \text{ ergs s}^{-1} \text{ cm}^{-2} \text{ Hz}^{-1} \text{ sr}^{-1}$, at low redshift and $J(\nu_0) = 1.0^{+3.8}_{-0.2} \times 10^{-22} \text{ ergs s}^{-1} \text{ cm}^{-2} \text{ Hz}^{-1} \text{ sr}^{-1}$ at high redshift.
- (2) The inclusion of blazars at $z < 1$, damped Ly α absorbers, or associated absorbers has no significant effect on the result.
- (3) Using information measured and gathered from the literature on each QSO's UV spectral index and solving for the HI ionization rate, yields $1.9 \times 10^{-13} \text{ s}^{-1}$ for $z < 1$ and $1.3 \times 10^{-12} \text{ s}^{-1}$ for $z > 1$. Solving directly for the parameters (A, B, z_c, S) in the HM96 parametrization of $\Gamma(z)$ using the HST/FOS data presented in Papers III and IV, combined with the high redshift,

ground-based data presented in Papers I and II, results in $(A, B, z_c, S) = (7.6 \times 10^{-13}, 0.35, 2.07, 1.77)$ for $1.7 < z < 3.8$.

(4) The $z < 1$ result is in agreement with the range of values of the mean intensity of the hydrogen-ionizing background allowed by a variety of local estimates, including $\text{H}\alpha$ imaging and modeling of galaxy HI disk truncations (Maloney 1993, Corbelli & Salpeter 1993, Dove & Shull 1994, Kutyrev & Reynolds 1989, Tumlinson et al. 1999). To within the uncertainty in the measurement, this result agrees with the one previous proximity effect measurement of the low redshift UV background (KF93). These results are consistent with calculated models based upon the integrated emission from QSOs alone (HM96) and with models which include both QSOs and starburst galaxies (Shull et al. 1999). The uncertainties do not make a distinction between these two models possible.

(5) The results presented here tentatively confirm the IGM evolution scenario provided by large scale hydrodynamic simulations (Davé et al. 1999). This scenario, which is successful in describing many observed properties of the low redshift IGM, is dependent upon an evolving $J(\nu_0)$ which decreases from $z = 2$ to $z = 0$. However, the low redshift UV background required to match the observations of the evolution of the Lyman α forest line density is larger than found from the data, indicating that structure formation is playing a role in this evolution as well. Our results and the work of others are summarized in Figure 1. We find some evidence of evolution in $J(\nu_0)$, though it appears that even larger data sets, especially at $z < 1$ and/or improved proximity effect ionization models will be required to improve the significance.

References

Bajtlik, S., Duncan, R. C., & Ostriker, J. P. 1988, *ApJ*, 327, 570
 Bechtold, J., Dobrzycki, A., Wilden, B., Morita, M., Scott, J., Dobrzycka, D.,
 Tran, K. V. 2001, in preparation (Paper III)
 Corbelli, E. & Salpeter, E. E. 1993, *ApJ* 419, 104
 Davé, R., Hernquist, L., Katz, N., & Weinberg, M. 1999, *ApJ*, 511, 521
 Dobrzycki, A., Bechtold, J., Scott, J., & Morita, M. 2001, in preparation (Paper
 IV)
 Dove, J. B. & Shull, J. M. 1994, *ApJ*, 423, 196
 Haardt, F. & Madau, P. 1996, *ApJ*, 461, 20 (HM96)
 Hu, E. M., Kim, T. -S., Cowie, L. L., & Songaila, A. 1995, *AJ*, 110, 2553
 Kulkarni, V. P. & Fall, S. M. 1993, *ApJ*, 413, L63 (KF93)
 Kutyrev, A. S. & Reynolds, R. J. 1989, *ApJ*, 344, L9
 Maloney, P. 1993, *ApJ*, 414, 41
 Scott, J., Bechtold, J., & Dobrzycki, A. 2000a, *ApJS*, 130, 37 (Paper I)
 Scott, J., Bechtold, J., Dobrzycki, A., & Kulkarni, V. 2000b, *ApJS*, 130, 67
 (Paper II)
 Shull, J. M., Roberts, D., Giroux, M. L., Penton, S. V., Fardal, M. A. 1999, *AJ*,
 118, 1450
 Tumlinson, J., Giroux, M. L., Shull, J. M., & Stocke, J. T. 1999, *AJ*, 118, 2148

Weymann, R. J., Jannuzi, B. T., Lu, L., Bahcall, J. N., Bergeron, J., Boksenberg, A., Hartig, G. F., Kirhakos, S., Sargent, W. L. W., Savage, B. D., Schneider, D. P., Turnshek, D. A., & Wolfe, A. M. 1998, *ApJ*, 506, 1

Williger, G. M., Baldwin, J. A., Carswell, R. F., Cooke, A. J., Hazard, C., Irwin, M. J., McMahon, R. G., & Storrie-Lombardi, L. J. 1994, *ApJ*, 428, 574